Record-breaking Meiyu rainfall around Yangtze River in 2020 regulated by the subseasonal phase transition of North Atlantic Oscillation

Boqi Liu[1], Yuhan Yan[1], Congwen Zhu[1*], Shuangmei Ma[1], Jianying Li[1,2]

[1] State Key Laboratory of Severe Weather and Institute of Climate System, Chinese Academy of Meteorological Sciences, Beijing 100081, China

[2] School of Environmental Studies, China University of Geosciences, Wuhan 430074, China

Corresponding author: Dr. Congwen Zhu (zhucw@cma.gov.cn)

Key Points:

- Sequential warm Meiyu front in mid–late-June and cold one in early–mid-July directly causes the record-breaking Meiyu rainfall in 2020
- The phase change of NAO leads to the alternation of circulation regime of East Asian summer monsoon from warm- to cold- front period
- Prediction skill of ECMWF subseasonal-to-seasonal model on the 2020 Meiyu rainband is higher in warm-front but lower in cold-front period

Abstract

In 2020, the long-persisting Meiyu season around the Yangtze River (YR) started in early-June and ended in mid–late-July. Its accumulated precipitation amount broke the record since 1961. We showed that the sequential warm and cold Meiyu front regulated by the North Atlantic Oscillation was responsible for this record-breaking Meiyu rainfall. From 11 to 25 June with the positive NAO, the interaction between South Asian High (SAH) and western Pacific subtropical high maintained a warm front to strengthen the rainband north of YR. Afterward, the coupling between SAH and mid-latitude Mongolian Cyclone induced a cold front, which retreated the rainband to the south of YR from 30 June to 13 July with the negative NAO. Although the ECMWF S2S successfully predicted the warm-front-related Meiyu rainband, it failed to forecast the Meiyu rainband in the cold-front period, suggesting a great challenge of the S2S forecast on Meiyu rainfall.

1. Introduction

Meiyu in China (also called Baiu in Japan and Changma in Korea) is the typical episode of the East Asian rainy season. It generally starts in early June and ends in mid-July. The zonally-elongated rainband of Meiyu covers the mid-lower reaches of the Yangtze River (YR), Korea, and Japan [*Tanaka*, 1992; *Tao and Chen*, 1987]. The Meiyu provides more than 40% of the total precipitation during East Asian summer monsoon (EASM) season [*Y H Ding and Chan*, 2005; *Oh et al.*, 1997]. The above-normal Meiyu rainfall has caused severe flooding to induce enormous loss of life and property in East Asian countries. Therefore, the researchers in East Asia has widely studied the multi-scale variability of Meiyu rainfall, and its prediction has become one of the most popular issues in the climate research [*Chen et al.*, 2017; *Y Ding et al.*, 2020; *Liu et al.*, 2020].

The Meiyu front is a quasi-stationary front with strong convective instability and rainstorm. It represents the interaction between warm-wet air mass from the tropics and cold-dry air mass from mid-high latitude. Its intensity and persistence directly determine the position and intensity of the Meiyu rainband [*Y Ding*, 1992; 2007; *Ninomiya*, 1984; 2000]. In the lower troposphere, the warm and wet air is transported by the lower-level southwesterly wind on the west of the western Pacific subtropical high (WPSH) [*Ha and Lee*, 2007; *Zhou and Yu*, 2005], whereas the cold and dry air embeds in the northerly wind on the west of the Mongolian Cyclone (MC, also termed cold vortex in Northeast China) [*He et al.*, 2007]. In the upper troposphere, the westerly jet and the South Asian High (SAH) upstream of the front could modulate either onset time or intensity of the Meiyu rainfall [*H Li et al.*, 2019; *Sampe and Xie*, 2010]. The year-by-year variation of the Meiyu rainfall not only depends on the El Nino–Southern Oscillation (ENSO) and its resultant SST anomaly in the Indian Ocean [*Kosaka et al.*, 2011; *B Wang et al.*, 2013], but also on the mid–high latitude wave trains over Eurasian continent [*H-H Hsu and Lin*, 2007; *Y Liu et al.*, 2019; *Z Wang et al.*, 2018]. On subseasonal timescale, the intraseasonal oscillation (ISO) of the EASM is the most crucial factor of the Meiyu activity [*Y Ding et al.*, 2020; *Huang et al.*, 2019; *Lau et al.*, 1988; *J Li et al.*, 2014; *Song et al.*, 2016; *B Wang and Xu*, 1997; *C Zhu et al.*, 2003]. Besides, the subseasonal variation of Meiyu rainfall can be modulated by the Madden-Julian Oscillation (MJO) [*X Li et al.*, 2018] or the summer North Atlantic Oscillation (NAO) [*Bollasina and Messori*, 2018].

In 2020, an extreme Meiyu rainfall attacked the mid-lower reaches of YR in China (Figure 1a). The accumulated precipitation from 11 June to 15 July reached 167.2mm to break its historical record since 1961 (Figure 1b), resulting in severe disasters in this area. Based on the position of the anomalous Meiyu rainband, we can divide this long-persisting Meiyu season into two subsections. The first period was from 12 to 25 June when the rainband got enhanced north of YR. Afterward, the anomalous rainband moved to the south of YR in the second period from 30 June to 13 July (Figure 1c). In particular, a record-breaking heavy rain, named "Heavy rain of July, Reiwa 2" by the Japan Meteorological Agency (JMA), hit the prefectures of Kumamoto and Kagoshima in the southern Japanese island of Kyushu on 4 July 2020 in the second period.

In history, the other two intense Meiyu rainfall around the YR took place in 1998 and 2016 following the super El Niño event, along with the significant MJO activity [*Shao et al.*, 2018; *C Zhu et al.*, 2003]. However, neither a super El Niño event nor an active MJO occurred in 2020. This situation brings substantial difficulties in the subseasonal-to-seasonal (S2S) prediction of the Meiyu rainfall this year. Thus, we are urgent to answer the following questions: (1) what caused this record-breaking Meiyu without either significant ENSO or active MJO? (2) Can the state-of-the-art S2S operational model predict the Meiyu rainfall in 2020? The present study used the 2479 in-situ rainfall observations provided by the National Meteorological Information Center in China. We described the circulation and thermal fields in the troposphere using the JRA-55 reanalysis dataset developed by the JMA, with a horizontal resolution of 1.25×1.25° and 37 standard isobaric surfaces from 1000 to 1 hPa [*Harada et al.*, 2016; *Kobayashi et al.*, 2015]. The real-time S2S production released by the ECMWF model was applied to examine the prediction skill of Meiyu rainfall this year (Please referred to the details in https://confluence.ecmwf.int/display/S2S/ECMWF+Model+Description+CY45R1). The climatological status was the arithmetic mean of each variable from 1981–2010. The region with the meridional gradient of the 700-hPa equivalent temperature higher than 2.0×10^{-5} K m^{-1} over

East Asia indicted the position of Meiyu front [*Fu and Qian*, 2011]. To reveal the subseasonal processes of Meiyu rainfall, we used a non-filtered method to calculate the subseasonal anomaly with a period of 10–60-day [*P-C Hsu et al.*, 2015].

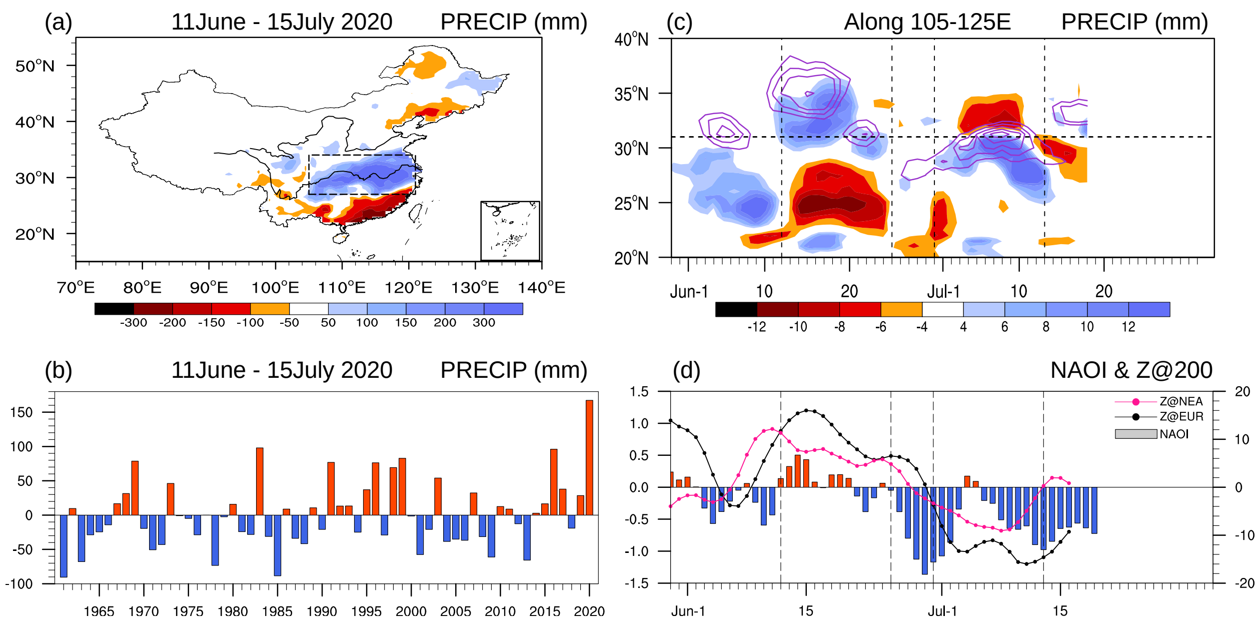

Figure 1. (a) Horizontal distribution of accumulated precipitation anomaly (mm) during the Meiyu season (11 June–15 July) in 2020. (b) Year-by-year variation of the accumulated precipitation anomaly during the Meiyu season averaged over [27°–34°N, 105°–121°E] indicated by the dashed box in (a). (c) Latitude-temporal cross-section of subseasonal anomalies of the daily-accumulated rainfall (shading, mm) and the Meiyu front (purple contours, starting from 1.0 with an interval of 1.0 × 10^{-5} K m^{-1}) averaged along 105°–125°E over East Asia. The Horizontal dashed line in (c) indicates the YR position. (d) Time series of subseasonal anomaly of the 200-hPa geopotential height averaged over Europe (EUR; 50°–70°N, 0°–40°E) (black line, gpm) and Northeast Asia (NEA; 30°–50°N, 110°–130°E) (pink line, gpm) and the normalized daily NAOI (bars).

2. Stepwise swing of Meiyu front and circulation regimes

The long-persisting Meiyu rainfall in 2020 features the stepwise swing of the Meiyu front and the circulation regimes on subseasonal timescale. In the first period, the Meiyu front gets enhanced near 35°N, where the rainfall increases considerably north of YR (Figures 1c and 2a). In the lower troposphere, the WPSH extents westward evidently to control South China and suppresses the local rainfall. The low-level southwesterly wind accelerates to bring more warm and wet air into the YR. In contrast, the anomalous northerly wind is relatively weak to the north of the front, indicating a warm front dominant in this period (Figure 2a). In the upper troposphere, a vast anomalous anticyclone generates over East Asia, corresponding to the anomalous northward shift and eastward extension of the SAH (Figure 2c). Therefore, the WPSH meets the SAH halfway to form a circulation pattern facilitating the above-normal Meiyu rainfall north of YR.

In the second period, the intensified Meiyu front and rainband retreats to the south of YR around 31°N (Figure 1c). An anomalous cyclone with vertically quasi-barotropic structure maintains over Northeast Asia (NEA), suggesting an enhancement of the mid-latitudinal MC (Figures 2b and 2d). On its west, the low-level northerly wind strengthens remarkably to bring more cold and dry air into the YR. On its east, the southerly wind intensifies dramatically to transport mass of moisture into the Kyushu island to support the "Heavy rain of July, Reiwa 2" (Figure 2b). Meanwhile, the anomaly center of WPSH settles to the south of Japan, in contrast to much weaker anomalies of the anticyclone and southerly wind over South China. It suggests a cold front determining the Meiyu rainband. In the upper troposphere, the more energetic MC with cold air mass is gearing with the southward extension of the SAH (Figure 2d), which retreats the Meiyu rainband to the south of YR. Thus, we can identify the above two periods as the warm- and cold- front period, respectively.

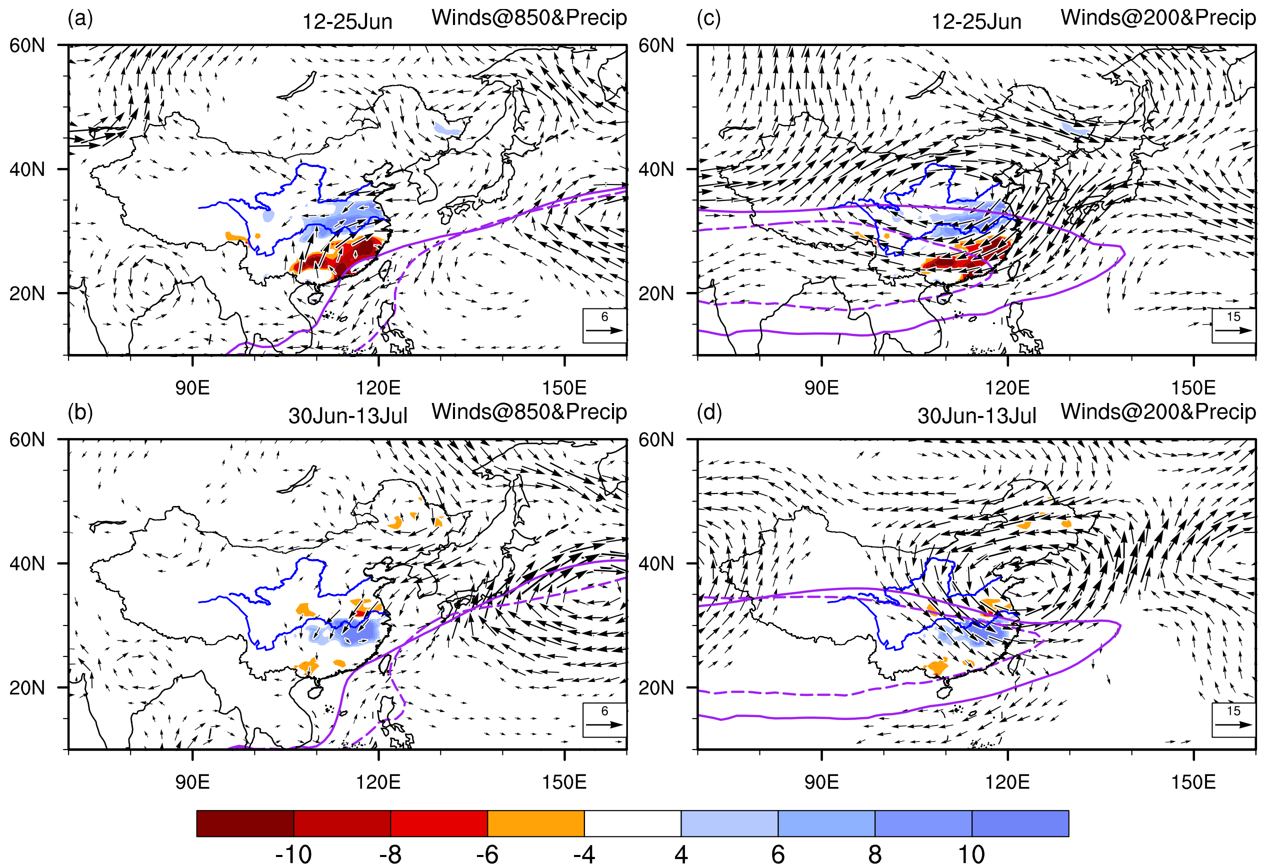

Figure 2. Subseasonal anomalies of atmospheric circulation (vectors, m s^{-1}) and rainfall (shading, mm day^{-1}) over East Asia in the two continuous rainfall stages of the 2020 Meiyu season. (a, c) warm-front period. (b, d) cold-front period. Left column: circulation at 850 hPa (wind speed higher than 1.0 m s^{-1} are plotted). Right column: circulation at 200 hPa (wind speed higher than 4.0 m s^{-1} are plotted). Purple curves in the left and right column respectively indicate the 152- and 1276- gpm contour of the 850- and 200- hPa geopotential height. Dashed and solid lines represent the climatological and the 2020 case, respectively.

3. Regulation by the phase transition of NAO

3.1 Linkage with NAO

The alternation of Meiyu warm and cold front with a distinct circulation regime follows the phase transition of NAO. The NAO firstly shows a positive phase in mid–June, it then enters an intense negative phase in late June and persists till late July (Figure 1d). In the warm-front period with positive NAO, an anomalous upper-level ridge exists over Europe, whose wave energy is emanated downstream along with the polar-front jet. It deepens the trough west of Lake Baikal and strengthens the NEA anticyclone in the upper troposphere (Figure 3a). The SAH thus tends to extent eastwards onto north of YR, presenting a negative anomaly of 200-hPa potential vorticity (PV) and anticyclone to the north of the anomalous Meiyu rainband (Figure 4a). Though partly compensated by the negative PV advection due to the anomalous PV, the positive PV advection induced by the anomalous northerly wind on the east of the SAH is prevailing during the warm-front period (Figures 4b and 4c). Firstly, this upper-level positive PV advection strengthens the ascending over the anomalous Meiyu rainband. The outflow then sinks over South China, where the low-level WPSH gets enhanced with a prominent westward extension, followed by more moisture supply to north of YR. The anomalies of Meiyu rainband and ascending further intensifies to establish a baroclinic structure of circulation, presenting the stronger low-level warm front and upper-level anticyclone north of YR (Figure 3c). Such positive feedback finally maintains a closed meridional circulation over East China to persist the anomalous Meiyu rainfall in the positive NAO phase.

When the negative NAO is prevailing in the cold-front period, Europe is beneath a striking deeper trough in the upper troposphere. It acts as a wave source to enhance the upper-level ridge over Northwest Asia and the cyclone over NEA with deep barotropic structure via a wave train between 40° and 60°N (Figure 3b). The NEA cyclone (i.e., stronger MC), represented by a remarkable positive PV anomaly at 200 hPa, brings more positive PV southward not only by the anomalous northerly wind but via the mean flow transport on the PV anomaly (Figures 4a–c). As a result, the high PV intrudes to the south of YR to develop the ascending over the anomalous Meiyu rainfall in this period (Figures 4b and 4c). The descending develops upstream of the NEA cyclone. It then diverges southward near the surface and merges into the ascending south of YR in early–mid-July (Figure 3d).

The physical linkage between NAO and anomalies of upper-level circulation over Europe and NEA can build a significant statistical relationship. The daily NAO index is significantly positively correlated with both the anomalous geopotential height over Europe (black line in Figure 1d) and NEA (pink line in Figure 1d), showing the temporal correlation coefficient (TCC) of +0.56 and +0.48, respectively. Both of them exceed the 95% confidence level in a two-tailed student t-test. However, the close relationship between NAO and NEA cyclone would vanish if we exclude the Europe ridge in a partial correlation analysis. Such a statistical relationship also holds in the July-mean fields on interannual timescale [*B Liu et al.*, 2019].

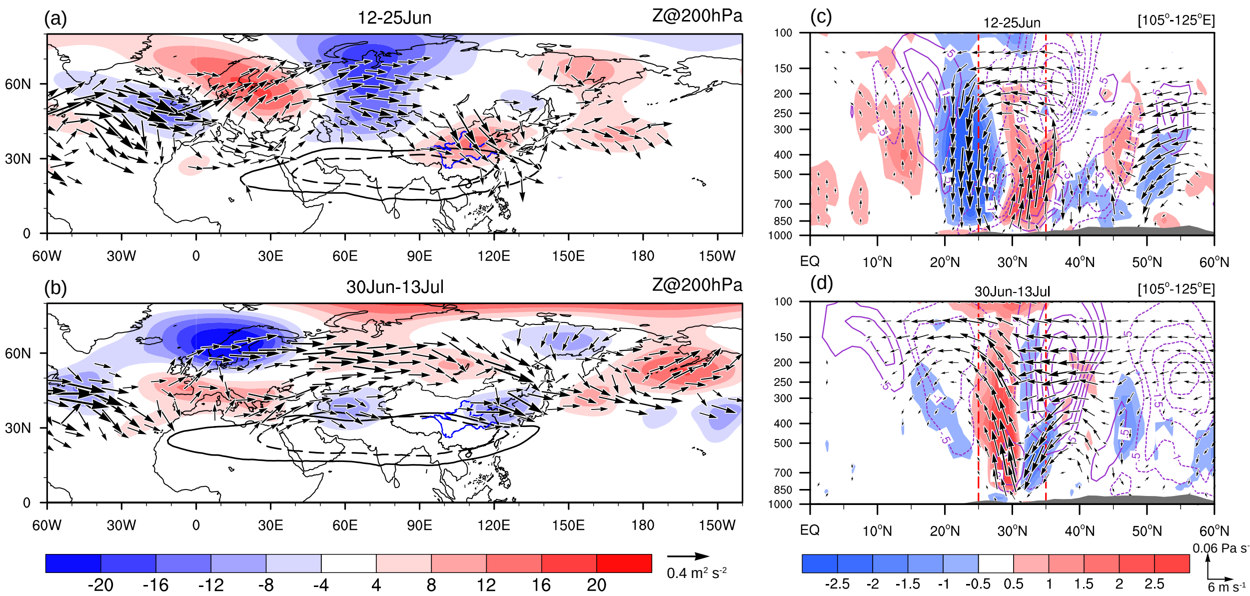

Figure 3. (left column) Horizontal distribution of anomalous geopotential height (shading, gpm) and wave activity flux (WAF) at 200 hPa (vectors, $m^2\ s^{-2}$) and (right column) 105°–125°E averaged pressure-latitudinal cross-section of subseasonal anomalies of the diabatic heating (shading, K day^{-1}), relative vorticity (purple contours, $10^{-5}\ s^{-1}$) and meridional circulation (vectors, see scales in the bottom right corner) in each rainfall stage of the Meiyu season in 2020. (a, c) warm-front period. (b, d) cold-front stage. Dashed and solid black lines in the left column indicate the 1276-gpm contour of the 200-hPa geopotential height in climatology and 2020, respectively. Gray shading in the right column denotes the topography. The WAF calculation follows *Takaya and Nakamura* [2001]'s formula.

Since the anomalous meridional advection contributes more to the temporal variation of the PV, air temperature and specific humidity than the anomaly of zonal advection (Figure not shown), we diagnose each component of the former to show how the variation of the upper-level circulation modulate the Meiyu front property and rainband position in 2020. In the warm-front period, the stronger WPSH extents westward under the influences of the eastward extension of the SAH and the positive PV advection in the upper troposphere. As a result of the warm-wet advection due to the stronger southwesterly wind over South China, the lower-tropospheric air becomes warmer and wetter to support the warm-front near the Meiyu rainband (Figures 4e and 4h). In contrast, the effect of the meridional advection anomaly due to the anomalous thermal and moisture fields is minimal (Figures 4f and 4i). In this way, the anomalous WPSH modulated by the anomaly of SAH determines the warm front and strengthens Meiyu rainfall north of YR in mid–late-June.

In the cold-front period, the positive PV advection induced by the more energetic MC becomes more remarkable. In the lower troposphere, the air tends to be colder and drier along with the YR because of the meridional cold and dry advection produced by the anomalous northerly wind (Figures 4e and 4h). The southward intrusion of the colder and drier air mass further increases the warm and wet advection over the anomalous Meiyu rainband by enlarging the anomaly of meridional temperature and moisture gradient, respectively (Figures 4f and 4i). Therefore, the cold-front and above-normal Meiyu rainfall persist south of YR in early–mid-July because of the extratropical MC anomaly in the mid-upper troposphere.

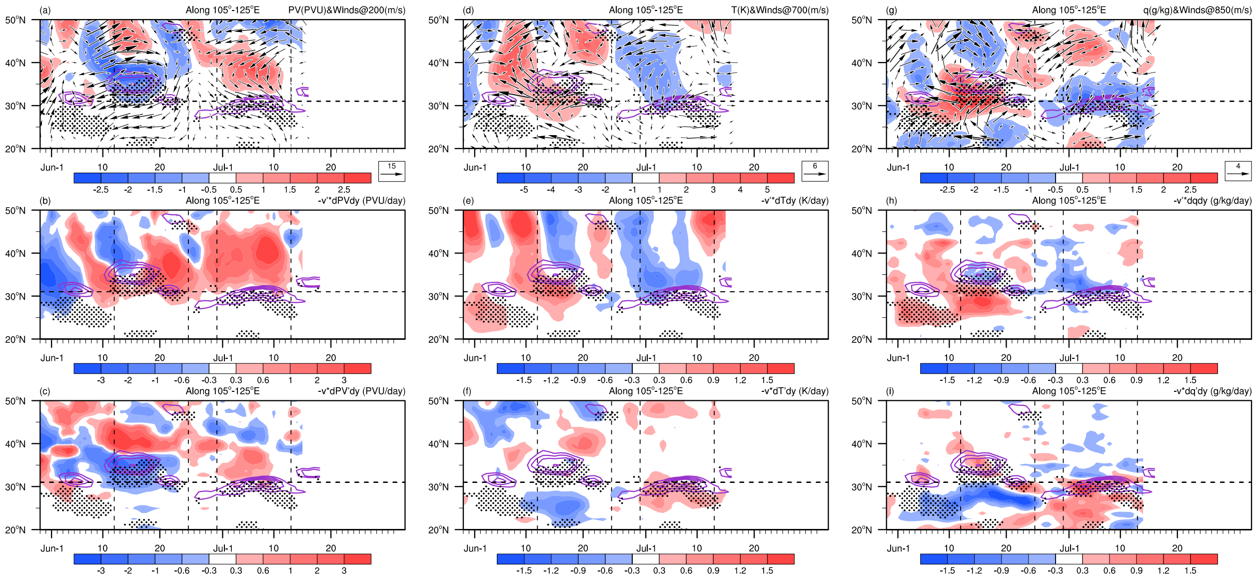

Figure 4. Left column: 105°–125°E-averaged latitude-temporal cross-section of the subseasonal anomalies of (a) the 200-hPa potential vorticity (shading, PVU) and horizontal winds (vectors, m s^{-1}), (b, c) the meridional PV advection (shading, PVU day^{-1}) due to anomalous meridional flow ($-v'\frac{\partial \overline{PV}}{\partial y}$) and PV ($-\bar{v}\frac{\partial PV'}{\partial y}$), respectively. Middle column: similar to the left column, but the shading and vectors in (d) are for the 700-hPa subseasonal anomalies of air temperature (K) and winds (m s^{-1}). and the shading in (e) and (f) denote the meridional temperature advection (K day^{-1}) induced by anomalous meridional flow ($-v'\frac{\partial \bar{T}}{\partial y}$) and temperature ($-\bar{v}\frac{\partial T'}{\partial y}$), respectively. Right column: similar as the left column, but the shading and vectors in (g) are for the 850-hPa subseasonal anomalies of specific humidity (g kg^{-1}) and winds (m s^{-1}), and the shading in (h) and (i) denote the meridional moisture advection (g kg^{-1} day^{-1}) induced by anomalous meridional flow ($-v'\frac{\partial \bar{q}}{\partial y}$) and specific humidity ($-\bar{v}\frac{\partial q'}{\partial y}$), respectively. Variables with bar and superscript indicate the climate-mean value and subseasonal anomaly, respectively. Purple contours and dots indicate the position of Meiyu front and large rainfall anomaly higher

than 4.0 mm day^{-1}, respectively.

3.2 Forecast skill of ECMWF S2S model

The prediction skill of the ECMWF S2S model on the Meiyu rainfall is distinct between the warm- and cold- front period in 2020. In the real-time forecast, the ECMWF S2S forecast can capture the features of Meiyu rainband in the warm-front period even 30 days in advance (Figures 5a and 5b). The median performance of the anomaly correlation coefficient (ACC) increases from 0.1 to above 0.4. The ensemble spread range gradually narrows with shortening of lead time, along with a stable range of root-mean-square-error (RMSE) between 6.0- and 8.0-mm day^{-1}. On the other hand, the prediction skill falls in the cold-front period (Figures 5a and 5b). Both the spatial structure and intensity of the Meiyu rainband are consistently poor performed among the individual ensemble members and ensemble mean, even at lead times within one week. These results indicate that the ECMWF S2S model has higher prediction skills on the Meiyu rainband when it is modulated by the WPSH and warm-wet air mass. However, the skill decreases dramatically when the mid-latitude circulation and cold-dry air mass maintains the Meiyu rainband.

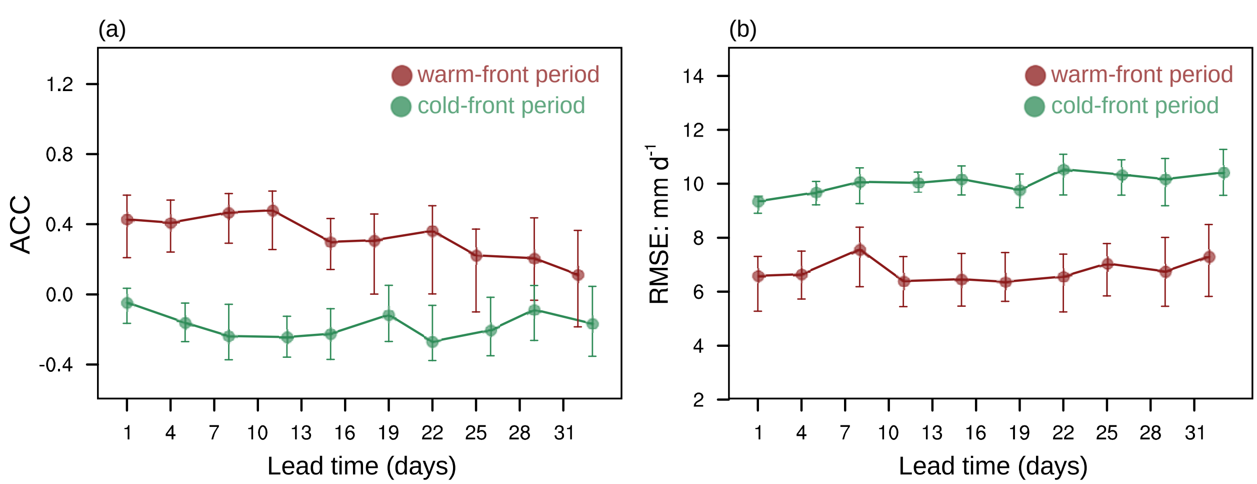

Figure 5. Box chart of (a) anomaly correlation coefficient (ACC) and (b) root-mean-square-error (RMSE, mm d^{-1}) between the ECMWF S2S forecast and observed inland rainfall anomaly in different lead times (up to 33 days) in the warm- and cold- front period over East China [20°−35°N, 105°−125°E]. The lead days are measured from the initialization time to 12 (30) June in the warm-front (cold-front) period. The metrics are calculated from 51 ensemble members (solid line) individually. The top, bottom, and junction points of the bars represent the 5th, 95th percentiles, and the median values, respectively.

4. Summary and discussion

A record-breaking Meiyu rainfall attacked East Asia in 2020. It has caused severe flooding to kill many residents in China and Japan. The present study has identified the warm- and cold-front subsection of this Meiyu season and ascribed the alternation of the circulation regime to the phase transition of the NAO. In mid–late-June, the positive NAO could induce the eastward extension of SAH and the westward extension of WPSH, leading to the stronger southerly wind over South China. The warm front thus gets enhanced and results in the anomalous Meiyu rainband north of YR. Afterward, the NAO enters its intense negative phase in early July. A wave train along the polar-front jet emerges to strengthen the mid-latitude MC, which not only enhances the ascending near the YR by dynamical procedure but maintains a stronger cold front along with the YR by the anomalous meridional temperature and moisture advection. Finally, the Meiyu rainband retreats south of YR in early–mid-July. The ECMWF S2S model shows a higher prediction skill on the warm-front-related rainfall, but it fails to predict the cold front-caused rainfall during the Meiyu season in this year. It suggests a great challenge still exists in the S2S dynamical prediction on the Meiyu rainfall, especially in the period when the mid–

high-latitude impact is dominant. The predictability of the extratropical circulation is much lower than either the MJO or the BSISO in the S2S forecast [*Hung et al.*, 2013]. It also limits the seasonal rainfall predictability of the EASM [*Kosaka et al.*, 2012].

One provoking question is why such a record-breaking event occurs in a weak ENSO environment comparing with 1998 and 2016. It is probably attributed to the global warming, which could increase the heavy rainfall near the YR in the Meiyu season [*C Zhu et al.*, 2012; *J Zhu et al.*, 2016]. Also, it may be associated with Arctic warming in June and July 2020. In particular, the strong negative NAO in late June 2020 is accompanied by the fast warming over North America in the Arctic cycle and the positive-to-negative transition of Arctic Oscillation. Further investigation is necessary for a comprehensive understanding of this record-breaking Meiyu flood over East Asia in 2020 on multiple timescales.

Acknowledgment

This work was jointly funded by the National Key R&D Program (2018YFC1505904), the National Natural Science Foundation of China (41830969,41775052, 41905076), the Basic Scientific Research and Operation Foundation of the Chinese Academy of Meteorological Sciences (CAMS) under grant 2018Z006. The authors declare that they have no conflicts of interest. The in-situ rainfall records were downloaded from http://data.cma.cn/en/?r=site/index. The JRA-55 reanalysis dataset was achieved at the National Center for Atmospheric Research, Computational and Information Systems Laboratory (https://doi.org/10.5065/D6HH6H41). The NAOI index was provided by NOAA/CPC from the website (https://www.cpc.ncep.noaa.gov/products/precip/CWlink/pna/nao.shtml). The ECMWF S2S production was downloaded from http://s2s.cma.cn/index.

References

Bollasina, M. A., and G. Messori (2018), On the link between the subseasonal evolution of the North Atlantic Oscillation and East Asian climate, *Climate Dynamics*, *51*(9), 3537-3557.

Chen, G., W. Sha, T. Iwasaki, and Z. Wen (2017), Diurnal Cycle of a Heavy Rainfall Corridor over East Asia, *Monthly Weather Review*, *145*(8), 3365-3389.

Ding, Y. (1992), Summer Monsoon Rainfalls in China, *Journal of the Meteorological Society of Japan. Ser. II*, *70*(1B), 373-396.

Ding, Y. (2007), The Variability of the Asian Summer Monsoon, *J. Meteor. Soc. Japan Ser. II*, *85B*, 21-54.

Ding, Y., P. Liang, Y. Liu, and Y. Zhang (2020), Multiscale Variability of Meiyu and Its Prediction: A New Review, *Journal of Geophysical Research: Atmospheres*, *125*(7), e2019JD031496.

Ding, Y. H., and J. C. L. Chan (2005), The East Asian summer monsoon: an overview, *Meteorology and Atmospheric Physics*, *89*(1-4), 117-142.

Fu, J.-L., and W.-H. Qian (2011), The Structure of a Typical Mei-Yu Front Identified by the Equivalent Temperature, *Atmospheric and Oceanic Science Letters*, *4*(2), 109-113.

Ha, K.-J., and S.-S. Lee (2007), On the interannual variability of the Bonin high associated with the East Asian summer monsoon rain, *Climate Dynamics*, *28*(1), 67-83.

Harada, Y., H. Kamahori, C. Kobayashi, H. Endo, S. Kobayashi, Y. Ota, H. Onoda, K. Onogi, K. Miyaoka, and K. Takahashi (2016), The JRA-55 Reanalysis: Representation of Atmospheric Circulation and Climate Variability, *J. Meteor. Soc. Japan Ser. II*, *94*(3), 269-302.

He, J., Z. Wu, Z. Jiang, C. Miao, and G. Han (2007), "Climate effect" of the northeast cold vortex and its influences on Meiyu, *Chinese Science Bulletin*, *52*(5), 671-679.

Hsu, H.-H., and S.-M. Lin (2007), Asymmetry of the Tripole Rainfall Pattern during the East Asian Summer, *Journal of Climate*, *20*(17), 4443-4458.

Hsu, P.-C., T. Li, L. You, J. Gao, and H.-L. Ren (2015), A spatial–temporal projection model for 10–30 day rainfall forecast in South China, *Climate Dynamics*, *44*(5), 1227-1244.

Huang, W.-R., P.-Y. Liu, J.-H. Chen, and L. Deng (2019), Impact of Boreal Summer Intra-Seasonal Oscillations on the Heavy Rainfall Events in Taiwan during the 2017 Meiyu Season, *Atmosphere*, *10*(4).

Hung, M.-P., J.-L. Lin, W. Wang, D. Kim, T. Shinoda, and S. J. Weaver (2013), MJO and Convectively Coupled Equatorial Waves Simulated by CMIP5 Climate Models, *Journal of Climate*, *26*(17), 6185-6214.

Kobayashi, S., Y. Ota, Y. Harada, and e. al. (2015), The JRA-55 Reanalysis: General specifications and basic characteristics, *J. Meteor. Soc. Japan*, *93*, 5-48.

Kosaka, Y., S.-P. Xie, and H. Nakamura (2011), Dynamics of Interannual Variability in Summer Precipitation over East Asia*, *Journal of Climate*, *24*(20), 5435-5453.

Kosaka, Y., J. S. Chowdary, S.-P. Xie, Y.-M. Min, and J.-Y. Lee (2012), Limitations of Seasonal Predictability for Summer Climate over East Asia and the Northwestern Pacific, *J. Climate*, *25*(21), 7574-7589.

Lau, K. M., G. J. Yang, and S. H. Shen (1988), Seasonal and Intraseasonal Climatology of Summer Monsoon Rainfall over Eeat Asia, *Monthly Weather Review*, *116*(1), 18-37.

Li, H., S. He, K. Fan, and H. Wang (2019), Relationship between the onset date of the Meiyu and the South Asian anticyclone in April and the related mechanisms, *Climate Dynamics*, *52*(1), 209-226.

Li, J., J. Mao, and G. Wu (2014), A case study of the impact of boreal summer intraseasonal oscillations on Yangtze rainfall, *Climate Dynamics*, 1-20.
Li, X., G. Gollan, R. J. Greatbatch, and R. Lu (2018), Intraseasonal variation of the East Asian summer monsoon associated with the Madden–Julian Oscillation, *Atmospheric Science Letters*, *19*(4), e794.
Liu, B., C. Zhu, J. Su, S. Ma, and K. Xu (2019), Record-Breaking Northward Shift of the Western North Pacific Subtropical High in July 2018, *Journal of the Meteorological Society of Japan. Ser. II*, *97*(4), 913-925.
Liu, Q., W. Zeng, G. Chen, and P. Guan (2020), Corridors of Mei-Yu-Season Rainfall over Eastern China, *Journal of Climate*, *33*(7), 2603-2626.
Liu, Y., Z. Ke, and Y. Ding (2019), Predictability of East Asian summer monsoon in seasonal climate forecast models, *International Journal of Climatology*, *39*(15), 5688-5701.
Ninomiya, K. (1984), Characteristics of Baiu Front as a Predominant Subtropical Front in the Summer Northern Hemisphere, *Journal of the Meteorological Society of Japan. Ser. II*, *62*(6), 880-894.
Ninomiya, K. (2000), Large- and meso-alpha-scale characteristics of Meiyu/Baiu front associated with intense rainfalls in 1-10 July 1991, *Journal of the Meteorological Society of Japan*, *78*(2), 141-157.
Oh, J.-H., W.-T. Kwon, and S.-B. Ryoo (1997), Review of the researches on changma and future observational study (kormex), *Advances in Atmospheric Sciences*, *14*(2), 207-222.
Sampe, T., and S. P. Xie (2010), Large-Scale Dynamics of the Meiyu-Baiu Rainband: Environmental Forcing by the Westerly Jet, *Journal of Climate*, *23*(1), 113-134.
Shao, X., S. Li, N. Liu, and J. Song (2018), The Madden–Julian oscillation during the 2016 summer and its possible impact on rainfall in China, *International Journal of Climatology*, *38*(5), 2575-2589.
Song, Z., C. ZHu, J. Su, and B. Liu (2016), Coupling Modes of Climatological Intraseasonal Oscillation in the East Asian Summer Monsoon, *Journal of Climate*, *29*, 6363-6382.
Takaya, K., and H. Nakamura (2001), A Formulation of a Phase-Independent Wave-Activity Flux for Stationary and Migratory Quasigeostrophic Eddies on a Zonally Varying Basic Flow, *J. Atmos. Sci.*, *58*, 608-627.
Tanaka, M. (1992), Intraseasonal Oscillation and the Onset and Retreat Dates of the Summer Monsoon over East, Southeast Asia and the Western Pacific Region using GMS High Cloud Amount Data, *Journal of the Meteorological Society of Japan. Ser. II*, *70*(1B), 613-629.
Tao, S., and L. Chen (1987), A review of recent research of the east Asian summer monsoon in China, in *Monsoon Meteorology*, edited by C.-P. Chang and T. N. Krishnamurti, pp. 60-92, Oxford Univ. Press, New York.
Wang, B., and X. Xu (1997), Northern Hemisphere Summer Monsoon Singularities and Climatological Intraseasonal Oscillation, *Journal of Climate*, *10*(5), 1071-1085.
Wang, B., B. Xiang, and J.-Y. Lee (2013), Subtropical High predictability establishes a promising way for monsoon and tropical storm predictions, *Proc. Natl. Acad. Sci. U. S. A.*, *110*(8), 2718-2722.
Wang, Z., S. Yang, N.-C. Lau, and A. Duan (2018), Teleconnection between Summer NAO and East China Rainfall Variations: A Bridge Effect of the Tibetan Plateau, *Journal of Climate*, *31*(16), 6433-6444.

Zhou, T.-J., and R.-C. Yu (2005), Atmospheric water vapor transport associated with typical anomalous summer rainfall patterns in China, *Journal of Geophysical Research: Atmospheres*, *110*(D8).

Zhu, C., T. Nakazawa, J. Li, and L. Chen (2003), The 30-60 day intraseasonal oscillation over the western North Pacific Ocean and its impacts on summer flooding in China during 1998, *Geophysical Research Letters*, *30*(18).

Zhu, C., B. Wang, W. Qian, and B. Zhang (2012), Recent weakening of northern East Asian summer monsoon: A possible response to global warming, *Geophysical Research Letters*, *39*(9).

Zhu, J., D. Huang, and T. Yang (2016), Changes of Meiyu system in the future under A1B scenario simulated by MIROC_Hires model, *Theoretical and Applied Climatology*, *123*(3), 461-471.